JOURNAL OF GEOPHYSICAL RESEARCH, VOL. 112, C12024, doi:10.1029/2007JC004336, 2007

Effect of wind variability on topographic waves: Lake Kinneret case

Elad Shilo,[1] Yosef Ashkenazy,[2] Alon Rimmer,[3] Shmuel Assouline,[4] Petros Katsafados,[5] and Yitzhaq Mahrer[1]

Received 11 May 2007; accepted 29 October 2007; published 29 December 2007.

[1] We studied the winter wind driven circulation in Lake Kinneret (northern Israel) using state of the art atmospheric (Regional Atmosphere Modeling System (RAMS)) and oceanic (Regional Ocean Modeling System (ROMS)) general circulation models. During winter the lake is completely mixed and mainly forced by the passage of synoptic weather systems. The lake's dynamic response was identified using various wind regimes. The response of the lake to a uniform wind stress resulted in the formation of a double-gyre circulation pattern. After removal of the wind stress, the double-gyre pattern slowly rotated cyclonically (with a time period of several days) around the lake perimeter, consistent with the pattern of the lowest-mode basin-scale topographic (vorticity) wave. The use of RAMS-simulated wind fields resulted in a less symmetric structure of the double-gyre pattern due to the presence of a curl in the wind field. Using various wind regimes to force the lake indicated that the presence of a positive or negative curl in the wind field might result in a shift in the topographic wave frequency to a higher or lower value, respectively. This result may be easily applied to motions on the geophysical scale. The currents predicted by RAMS-ROMS agree well with measured data near the center of the lake. Forcing the model with a spatially uniform wind field constructed from a single station resulted in poor agreement with the observed currents, indicating the importance of the wind field spatial pattern.

Citation: Shilo, E., Y. Ashkenazy, A. Rimmer, S. Assouline, P. Katsafados, and Y. Mahrer (2007), Effect of wind variability on topographic waves: Lake Kinneret case, *J. Geophys. Res.*, *112*, C12024, doi:10.1029/2007JC004336.

1. Introduction

[2] Wind induced currents play a key role in the dynamics of aquatic ecosystems. The transport of dissolved substances, the mixing of the lake water column, and the resuspension of bottom sediments are largely influenced by these currents [*Serruya*, 1975; *Podsetchine and Schernewski*, 1999]. Information related to wind driven circulation patterns is also used in modeling phytoplankton patchiness in lakes [e.g., *Verhagen*, 1994]. Reducing the possibility of uncertainties in a lake's response to wind-forcing will provide more accurate conditions for further studies concerning water quality issues. However, the identification of the induced circulation pattern should include the wind-forcing period accompanied by a free period.

[3] The response of a depth-variable, homogenous, f-plane lake to the action of a uniform wind stress often consists of downwind flow occurring at the shallower, nearshore areas with an upwind return flow at the deeper parts of the lake. The streamlines of the flow field form two counterrotating circulation cells, known also as the double-gyre pattern: a counterclockwise gyre is formed to the right of the wind and a clockwise gyre to the left [*Csanady*, 1973; *Bennett*, 1974; *Simons*, 1980]. The formation of this classic double-gyre pattern, which requires the occurrence of a flow across contours of constant f/h (f is Coriolis parameter and h the depth) releases/gains relative vorticity. This effect provides a restoring tendency for topographic waves over a slope (for more details, see *Rhines* [1969]). After removal of the wind stress, there is a cyclonic propagation of the double-gyre pattern around the basin with a characteristic period corresponding to the lowest-mode topographic (vorticity) wave of the basin [*Csanady*, 1976; *Raudsepp et al.*, 2003].

[4] Topographic waves belong to the so-called second class motions. First class motions are long gravity waves which cause significant disturbance of the free surface. The essence of the first class motion is the alternation between potential and kinetic energies [*Ball*, 1965], and typical frequencies of these motions are generally much higher than the local Coriolis parameter, f. Therefore it is assumed

[1]Department of Soil and Water Sciences, Hebrew University of Jerusalem, Rehovot, Israel.
[2]Department of Solar Energy and Environmental Physics, Jacob Blaustein Institutes for Desert Research, Ben-Gurion University of the Negev, Sede Boqer, Israel.
[3]Yigal Alon Kinneret Limnological Laboratory, Oceanographic and Limnological Research, Migdal, Israel.
[4]Department of Environmental Physics and Irrigation, Institute of Soils, Water and Environment Sciences, Volcani Center, Agricultural Research Organization, Bet Dagan, Israel.
[5]Laboratory of Meteorology, Department of Applied Physics, National and Kapodistrian University of Athens, Athens, Greece.

0148-0227/07/2007JC004336$09.00

that the existence of these motions is not related to Earth rotation. The second class of oscillatory motions does not significantly disturb the free surface; the motion is essentially rotational and is affected by the Earth's rotation. Second-class motion dynamics depend on a gradient of potential vorticity in the fluid at rest that is provided by variations in the equilibrium depth of the lake. Typical frequencies of these waves are considerably lower than f [*Ball*, 1965; *Rao and Schwab*, 1976; *Birchfield and Hickie*, 1977]. A prominent feature of a topographic wave is the slow cyclonic rotation of the current vector at the lake center, in a parabolic-like depth configuration [*Saylor et al.*, 1980]. The presence of the lowest-mode basin-scale topographic wave has been suggested as being causative of the low-frequency current or temperature fluctuations observed in lakes of differing size, for example Lake Ontario [*Csanady*, 1976], Southern Lake Michigan [*Saylor et al.*, 1980], Lake Lugano and Lake Zurich [*Mysak*, 1985a, 1985b]. By analysis of observations and by using an idealized lake model, *Csanady* [1976] connected between several flow reversal episodes in Lake Ontario, and the appearances of barotropic topographic wave. The estimated time period for the wave propagation was 12–16 days. *Saylor et al.* [1980] observed low-frequency oscillatory motions in the southern basin of Lake Michigan. The current vector rotates cyclonically at the center of the basin and anticyclonically elsewhere with a time period of about four days. Their analysis showed that the wave frequency is sensitive to a lake's shape and its bathymetry. *Mysak* [1985a, 1985b] suggested an analytical method to calculate the topographic wave frequency. The description of the effect of bathymetry and depth profile on topographic wave frequency was more detailed than that of *Saylor et al.* [1980] and an agreement was achieved with time periods of low-frequency currents oscillations in lakes such as Lake Lugano, Lake Zurich, and Lake Michigan.

[5] While the existing information regarding the effect of first class motions on processes in lakes seems to be more complete, there is still a lack of knowledge regarding the so-called topographic waves (see review by *Wüest and Lorke* [2003]). *Stocker* [1988] stated that a remarkable amount of kinetic energy of water motions in ocean bays and lakes is embodied in long-periodic (topographic) waves. However, according to *Wüest and Lorke* [2003], their potential role in the internal energy cascade is still to be shown. Perhaps an example of the importance of topographic waves was demonstrated in the observations of *Rao et al.* [2004] in southern Lake Michigan. They pointed out that the combination of direct wind forced currents and propagated vorticity waves generates significant offshore transport and thus provides a mechanism for exchange of materials between nearshore and offshore.

[6] In a natural environment the wind field above a lake is likely to be spatially nonhomogenous and this in turn may have a significant effect on the evolution of large-scale lake circulation. Several studies have reported that spatially nonhomogenous wind caused the formation of a single circulation cell instead of the topographic double-gyre pattern (for a detailed description, see *Schwab and Beletsky* [2003], and *Rubbert and Kongeter* [2005]). If, for example, a single circulation cell forms and the flow roughly follows the depth contours, we would not expect the appearance of a basin-scale topographic wave. Thus identification of a lake's response to realistic wind conditions is important since it affects the free response of the lake (after cessation of the wind).

[7] The main goal of this study is to investigate the role of the spatial and temporal variability of the wind field on the large-scale circulation pattern in a homogenous lake. We focus our attention on a lake that is surrounded by a complex terrain, where the forcing wind field is already known to be highly variable. Hence a secondary goal is providing a physically sound description of the wind field to be use as a top boundary condition for the lake. Lake Kinneret (northern Israel) served as an excellent case study to gather information about these responses under variable wind conditions. In section 2, we provide some physical background for Lake Kinneret as well as a brief description of past observations and modeling efforts. We then describe the two test cases under consideration, and the hydrodynamic and the meteorological numerical models (section 3). In section 4, a physical explanation for the effect of wind variability on the lake response is provided. Summary and conclusion are given in section 5.

2. Lake Kinneret Circulation

[8] Lake Kinneret is a warm, monomictic lake located at the northern end of the Afro-Syrian Rift Valley, in Northern Israel. It is the only substantial free-water reservoir of Israel, supplying about 25% of the national water consumption. The lake is situated at 32°42′–32°55′ N latitude; 35°31′–35°39′ E longitude; it is 22 km long on the N-S axis and 12 km wide on the W-E axis. At a water level of 209 m below mean sea level (MSL), the lake surface area is 170 km^2, its volume is 4.3×10^6 m^3, the maximum depth is equal to 43 m, and its mean depth is 26 m [*Serruya*, 1975]. The main streamflow into the lake is the Upper Jordan River situated at the northernmost part of the lake. The main outlet is the National Water Carrier which pumps from the lake's northwest part near Tabgha (see Figure 1). The main natural outlet, which is usually blocked, is the Lower Jordan River at the southernmost point of the lake. The lake is roughly elliptical with a parabolic-like depth profile (e.g., depth contours parallel to shore line; see Figure 1), a shape that makes it most suitable for verification of analytical studies which relate to lake circulation.

[9] During the last four decades the circulation in Lake Kinneret has been the subject of intensive research. The work of *Serruya* [1975] summarized three consecutive years (1972–1974) of measurements in the lake. It indicated that when the lake was stratified, a dominant cyclonic circulation occurred, mainly owing to the passage of a strong westerly wind, such as occurs during the summer and most of the spring and autumn. Occasionally, anticyclonic circulation events were observed during particular days in autumn or spring when very weak winds prevailed. During the complete mixing period, *Serruya* [1975] identified a cyclonic circulation resulting from the passage of easterly winter wind storms. Occasionally, anticyclonic circulation events were observed during days with wind speed values below 3.0 m s^{-1}, usually after a wind storm dissipation; *Serruya* [1975] measurements were conducted at the lake

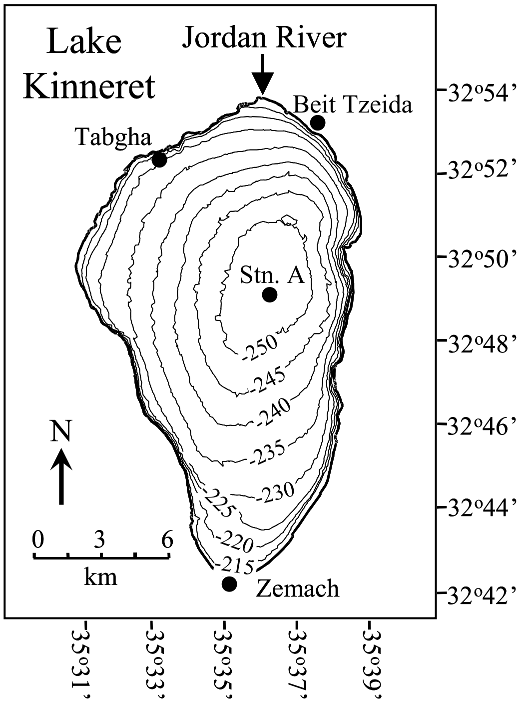

Figure 1. Lake Kinneret bathymetric map and location of meteorological stations at Zemach, Tabgha, Beit-Tzeida, and Station A. Altitudes are in meters below MSL.

periphery. The above findings motivated us to expand the study on Lake Kinneret dynamics.

[10] So far, the main observational and theoretical efforts in Lake Kinneret hydrodynamics were directed at the physical phenomena which occur during the stratification period from April to December [e.g., *Ou and Bennett*, 1979; *Antenucci et al.*, 2000; *Pan et al.*, 2002]. However, a review of the findings of studies from this period reveals that there are still several uncertainties which we will briefly describe below.

[11] Several modeling studies investigated the stratified Lake Kinneret response to spatially uniform wind stress. *Ou and Bennett* [1979] proposed that the summer circulation in the lake is dominated by an internal Kelvin wave which develops at the thermocline (the internal Rossby radius of deformation during summer is approximately 5 km while the barotropic radius is $\sim$200 km). Later, the presence of an internal Kelvin wave and internal Poincare waves were identified by *Antenucci et al.* [2000]. They suggested that the occasional anticyclonic circulation observed by *Serruya* [1975] was due to the dominance of Poincare waves. However, Poincare waves occur at the thermocline plane when the lake is stratified. Therefore their suggestion does not explain the observations of anticyclonic circulations during winter, when the lake was completely mixed.

[12] The analysis based on spatially uniform wind-forcing raised another uncertainty. Results of wind measurements [*Serruya*, 1975; *Asculai et al.*, 1984; *Assouline and Mahrer*, 1996] and simulations using numerical meteorological models [*Alpert et al.*, 1982; *Avissar and Pan*, 2000] had clearly indicated that the summer wind field above the lake has a large spatial variability, mainly due to the complex topography around the lake. *Pan et al.* [2002] used simulated surface wind fields employing a three-dimensional (3D) meteorological model to force a 3D hydrodynamic model of Lake Kinneret. They suggested that the spatial variability in the wind field is the dominant mechanism affecting the lake's summer circulation, and showed that the lake's mean cyclonic circulation is generated directly by the wind stress curl during the passage of the daily Mediterranean Sea Breeze (MSB) (10–15 m s^{-1}) over the lake. The MSB is a mesoscale meteorological phenomenon in the form of a west wind usually arriving at noon (1300–1400 local standard time (LST)) and relaxing in the late evenings [*Alpert et al.*, 1982]. The numerical experiments of *Pan et al.* [2002] also suggested that the summer circulation due to internal waves is minor. Therefore the mechanism which stands behind the flow reversal events during summer is still under question. *Laval et al.* [2003] confirmed the interpretation of *Pan et al.* [2002] by demonstrating that a spatially varying wind field is necessary to achieve good agreement between the modeled and observed lake circulation patterns as well as the phase and magnitude of internal waves.

[13] During the period (December to March) the homogenous lake is forced by a wind regime that is significantly different from the summer regime. Winter winds are characterized by the passage of large-scale synoptic weather systems above the entire region (eastern Mediterranean). This can generate wind storms above the lake, which can last between 12 and 48 hours, followed by several days of calm winds with no specific direction. Strong winds above the lake occur mainly owing to the presence of two distinctly different synoptic weather systems. The first is the high pressure system centered above Turkey usually resulting in an easterly storm above Lake Kinneret. The second concerns the passage of a low-pressure system (Cyprus low) coming from the eastern coast of the Mediterranean Sea and heading northeast. This results in the formation of a strong southwest wind above the lake. The interaction of these strong winds with the complex terrain that surrounds Lake Kinneret generates a significant spatial variability in the wind field which in turn has an effect on the lake's circulation.

[14] Despite the importance of understanding physical processes occurring during the winter, only the steady state, linear barotropic response of the lake under different boundary conditions has been examined. The formation of a double-gyre circulation pattern has been demonstrated using spatially uniform wind [*Serruya et al.*, 1984]. These results indicated that the formation of a steady single-cell cyclonic circulation is possible when forcing the lake by a theoretical easterly wind field with decreasing magnitude from north to south. It also served as an explanation for the observations of *Serruya* [1975] that the passage of easterly winter storms over the lake resulted in a cyclonic circulation pattern. Recent data (from January 2004), collected near the center of the lake show several events in which a slow cyclonic rotation of the current vector was observed, immediately after cessation of a wind storm. On the basis of past evidence, we suggest here that this cyclonic rotation can be linked to the presence of a lowest-mode topographic wave produced by the storm that persists for several days.

[15] Lake Kinneret is suitable to test the theory of topographic waves under realistic situations. The approximate ellipsoidal shape of the lake together with its approximate parabolic-like bathymetry makes it suitable for validating the topographic wave theory. In addition, the richness of the wind pattern (caused in part by the complex topography that surrounds the lake) enables examination of topographic wave existence and pattern subject to various scenarios. Thus the conclusions of this study may help to identify topographic waves and their characteristics in lakes with less idealized bathymetry. The uniqueness of this study compared to previous studies that identified topographic waves [e.g., *Raudsepp et al.*, 2003] lies in the spatial variability of wind-forcing, together with the almost idealized bathymetry of the lake, a fact that helped us to study in detail the reaction and formation of topographic waves under different wind patterns. More specifically, we show that the frequency of the topographic waves may significantly decrease or increase according to the spatial and temporal variability of the wind field. Better understanding of the homogenous lake system may also help us to clarify the findings concerning water motions during the stratification period, especially those that were observed during days with no wind.

3. Methodology

[16] In the present study we used a 3D state-of-the-art numerical hydrodynamic model (Regional Ocean Model System (ROMS)) [*Shchepetkin and McWilliams*, 2005] to study the dynamic response of the homogenous winter lake to the action of two typical wind storm cases: I, an easterly wind storm, and II, a southwesterly wind storm. The response of the lake to the passage of an easterly wind storm (case I) was studied first using a theoretical spatially uniform wind, impulse type in time. We then used wind fields simulated by a high resolution state of the art numerical meteorological model (Regional Atmospheric Modeling System (RAMS)) [*Pielke et al.*, 1992]. To study the effect of the southwesterly wind storm (case II), the lake model was forced with wind values from single station observations (i.e., temporally variable but spatially uniform wind fields). The effect of spatial variability of the wind field was then addressed by using simulated wind fields for the same period with the aid of the meteorological model.

3.1. Hydrodynamic Model ROMS

[17] ROMS is a free-surface, hydrostatic, finite difference, primitive equation model that uses orthogonal curvilinear coordinates in the horizontal direction. In the vertical direction, the primitive equations are discretized over variable topography using stretched terrain-following coordinates [*Song and Haidvogel*, 1994]. The horizontal grid for this application was composed of 36×58 grid cells 400×400 m^2 in size, covering an area of about 14×23 km. Twenty vertical layers were used in the simulations, providing high vertical resolution for shallow areas. High-resolution bathymetry data (400×400 m^2) was used. To avoid numerical errors in calculating horizontal pressure gradients, the bathymetry was smoothed such that the relative depth gradient $\nabla h/h \leq 0.2$ was satisfied everywhere in the basin where h is the water depth at rest [*Beckman and Haidvogel*, 1993]. Vertical viscosity and diffusivity were calculated using the nonlocal K-Profile Parameterization (KPP) scheme [*Large et al.*, 1994]. The background values of vertical viscosity and horizontal diffusion were 10^{-5} m^2 s^{-1} and 5 m^2 s^{-1}, respectively. The components of the currents normal to the boundary were set to zero and all the boundaries including the surface were assumed to be thermally insulated. For the depth-averaged currents a quadratic friction law was assumed with a dimensionless drag coefficient of 5×10^{-4}. Free slip conditions were imposed for the lateral boundaries. During the simulations, the lake temperature was kept constant at a representative value for the Lake Kinneret winter period (16°C). The lake water level at rest was at 208.9 m below mean sea level indicating a maximal depth of ~43 m. Since Lake Kinneret is a fresh water lake the salinity of the lake was assumed not to affect the lake's dynamics.

3.2. Meteorological Model RAMS

[18] We used the Colorado State University (CSU) Regional Atmospheric Modeling System (RAMS, version 6.0) in this study. RAMS is a multipurpose 3D versatile numerical prediction model designed to simulate atmospheric systems. It is constructed around a full set of equations in terrain following coordinates system, which governs atmospheric motions. The equations are supplemented with optional parameterizations for turbulence, radiation, thermodynamics, cloud microphysics, soil type, and vegetation.

[19] Two representative cases of winter wind storms were simulated and then used to force the lake model. For each case, the model configuration was chosen according to the synoptic conditions that prevail during the relevant period.

3.2.1. Case I Easterly Wind Storm

[20] A 30-hour simulation was performed in order to provide the passage of an easterly storm above Lake Kinneret during 01–03 January 2001 (started at 01 January 0000 Greenwich Mean Time (GMT)). During this period, a high-pressure system was centered above Turkey, causing moderate easterly winds above Israel. Weather conditions during this period were characterized by a clear sky without precipitation and a continuous rise in the air temperature. Preliminary tests show that the best results were achieved using *Mahrer and Pielke*'s [1977] scheme for calculating short and long wave radiation without activating the cloud microphysics package. The model was configured with three nested grids, with horizontal cell size of 16, 4, and 1 km, respectively; previous studies recommended configuring the model according to the case under consideration. (Note that in the second case described below the grid configuration is different.) The two inner grids were centered above Lake Kinneret while the location and the extent of the coarser grid were chosen after a series of preliminary tests that were aimed to achieve an effective update of the mesoscale model without interference with the dynamic evolution [see *Alpert and Krichak*, 1996]. Details of the three grids are given in Table 1. All three grids had 40 vertical layers. Owing to the steep topography around Lake Kinneret, the first layer near the surface was approximately 100 m thick (corresponding to a first model level of 50 m above the surface) and the thickness of the higher layers was gradually increased to a maximal value of 1200 m. Simulations using smaller vertical spacing near

Table 1. RAMS Grid Configuration Parameters for Case I (Three Grids) and Case II (Four Grids)[a]

Grid	NX	NY	Cell Size, km	W-E Distance km	N-S Distance, km	Location of the Grid Center, Latitude, deg	Location of the Grid Center, Longitude, deg
				Case I			
1	68	100	16	1088	1600	35.32	38.10
2	98	98	4	392	392	32.82	35.59
3	50	50	1	50	50	32.82	35.59
				Case II			
1	66	66	27	1782	1782	32.82	35.59
2	47	47	9	423	423	32.82	35.59
3	35	35	3	105	105	32.82	35.59
4	50	50	1	50	50	32.82	35.59

[a]The model parameters include the number of grid points in x and y directions, the horizontal grid spacing, and the area covered by each grid. NX denotes number of grid points in the x direction. NY denotes number of grid points in the y direction.

the surface yielded unrealistic results (i.e., large errors in surface temperature field). In meteorological models that use terrain following coordinate system numerically inconsistent approximation of the horizontal gradients/terms may occur in the presence of very steep topography [see *Mahrer*, 1984] which is the case of Lake Kinneret surroundings.

[21] Land-use data for all grids and topography for grids 1 and 2 were derived from 1/120 degree ($\sim$1 km) resolution data from the United States Geological Survey (USGS). High resolution topography data (250 m) from the geographical information system of the Hebrew University of Jerusalem in Israel were implemented into the finest grid (grid 3). Vertical and horizontal diffusion were calculated using the *Mellor and Yamada* [1982] 2.5 level closure and by the Smagorinski-type scheme, respectively.

3.2.2. Case II Southwesterly Storm

[22] The second simulation covered 72 hours starting at 22 January 2004 0000 GMT. The aim of this simulation was to describe a wind storm resulting from the passage of a synoptic Cyprus low above Israel. This relatively deep, low pressure system initiated a southerly wind flow above Israel at 23 January 2004. During the following two days, this low pressure system moved along a northeasterly axis with the wind direction turning southwesterly. The weather was characterized by a continuous decrease in the air temperature and the formation of precipitation above the northern and central part of Israel. Preliminary tests showed that the best results (focusing on the surface wind fields) were achieved by using the *Harrington* [1997] scheme to calculate short and long wave radiation. The microphysics package was activated at the highest level (3) and the Kain-Fritsch convection scheme [*Kain and Fritsch*, 1993] was activated for the coarse grid. The model was configured using four nested grids with cell sizes of 27, 9, 3, and 1 km, respectively, centered above the middle of the lake. More details of the four grids used for this simulation are given in Table 1. The vertical configuration was identical to the first case described above. Land-use data for all grids and topography for grids 1, 2, and 3 were derived from 1/120° ($\sim$1 km) resolution data from the United States Geological Survey (USGS) while the high resolution topography data used in the finest grid was as in the first case described above (250 m). Initial and boundary conditions of the European Centre for Medium-Range Weather Forecasts (ECMWF) reanalysis data (horizontal resolution of 0.5° Lat/Lon) were assimilated into the model. Boundary conditions were updated every six hours.

[23] Wind values as simulated by RAMS at 50 m height (top of the surface layer) were extrapolated downward by the logarithmic wind profile to a standard 10 m height with a roughness height of 2×10^{-4} m. The simulated wind fields (1 km $\times$ km) were (spline) interpolated to the lake grid of 0.4×0.4 km.

3.3. Numerical Experiments With ROMS

[24] The dynamic response of the homogenous Lake Kinneret (LK) was investigated using two representative wind-forcing regimes as described in the previous subsection. We performed a total of four experiments that are described below. The first and second experiments (1 and 2 in Table 2) were designed to study the lake's response to the action of a strong easterly wind while the third and fourth experiments (3 and 4 in Table 2) were designed to simulate the lake's response during the passage of a Cyprus low above the region (22–26 January 2004). The experiments are as follows.

[25] 1. In the first experiment a spatially uniform easterly wind field was used in ROMS simulation; the wind magnitude was 10 m s^{-1} for the first 12 hours, then the wind was switched off and the simulation continued to complete four days. This case represents a reference experiment.

[26] 2. In the second experiment, wind fields simulated by the meteorological model RAMS (case I) were used to force ROMS for the first 30 hours. For the rest of the simulation (66 hours), the wind stress was set to zero; altogether four days of simulation were performed. The purpose of this simulation was to examine the lake's response to the passage of an easterly storm of approximately 12 hours with considerable spatial variability in the wind field.

[27] 3. In the third experiment, spatially uniform but temporally variable wind fields were constructed using values from single station observations located near the center of the lake (Station A; see Figure 1) and used to force ROMS during the first 72 hours. The simulation continued without any wind up to 120 hours (five days).

Table 2. Numerical Experiments With ROMS: Wind-Forcing Types

Experiment	Wind Field (Spatial)	Wind Field (Temporal)	Duration of Wind-Forcing (Mag. > 3 m s^{-1}), hours	Type of Wind Field	Duration of ROMS Simulation, hours
1	uniform	uniform	12	theoretical	96
2	variable	variable	12	simulated using RAMS	96
3	uniform	variable	72	single station observations	120
4	variable	variable	72	simulated using RAMS	120

[28] 4. The fourth experiment was similar to the third, except that the first 72 hours wind fields were those simulated by RAMS (starting at 22 January 2004 0000 GMT). Table 2 summarizes the different wind-forcing types applied in the four experiments.

3.4. Observations

3.4.1. Current Observations

[29] Vertical profiles of horizontal current velocities were measured by the Kinneret Limnological Laboratory (KLL), using 300 kHz ADCP (Teledyne RD Instruments) located at different points during the two different periods. For the period of January 2001 (case I) the ADCP was located at a shallow, nearshore, region (Fuliya site; see Figure 6 in section 4.4 for location) and the measured depth was between 2.5 and 7.5 m. For the period of January 2004 (case II), the ADCP was located at the deepest part of the lake (Station A, Figure 1). Current velocities were sampled at 0.1 Hz frequency and averaged over a one hour interval.

3.4.2. Meteorological Observations

[30] Wind data were measured in four different locations around the lake perimeter and above the lake surface. These include the Zemach onshore station (ZE) near the southern shore of the lake, Beit Tzeida (BT) onshore station near the east corner of the northern shore, Tabgha (TB) offshore station at the western north side of the lake, and the offshore station A (Station A), located on a raft near the lake center (Figure 1). The wind data were provided by a joint agreement between the Israeli Meteorological Service (IMS) and KLL. For case I, wind data were available from three sites (TB, ZE and BT) while for case II, data from Station A were also available. In all stations, measurements of wind speed (m s^{-1}) and wind direction (degrees) were taken by a YOUNG wind monitor MA-05106. Measurements were taken each second at 10 m above ground or water level, and averaged over a ten minute interval. Later the data were averaged over a one hour period.

4. Results and Discussion

4.1. Lake Response to a Theoretical Easterly Wind Storm

[31] The depth integrated currents after the action of a spatially uniform easterly wind field (see Experiment 1, Table 2) are depicted in Figures 2a–2d. A clear topographic double-gyre pattern was developed (Figure 2a). As expected, at shallow depths the flow was directed downwind, parallel to the depth contours while in the deeper, central part of the lake, an upwind return flow formed, causing water particles to cross depth contours. A cyclonic gyre was located at the northern and central parts of the lake while an anticyclonic smaller gyre covered the southern part of the lake. The free period (i.e., the period with no wind after the action of the wind stress) was characterized by a cyclonic propagation of the double-gyre pattern as depicted in Figures 2b–2d. This type of motion is quite similar to the characteristics of the lowest mode basin-scale topographic wave [*Ball*, 1965].

[32] Immediately after cessation of the wind, the kinetic energy of the flow along the west coast was relatively higher than that in other parts of the lake as can be seen from Figure 2a. During the free period, friction at the bottom of the lake reduced the overall kinetic energy. However, it is interesting to note that the magnitude of the currents (kinetic energy) in the southern part was relatively higher than those of the northern part of the lake (Figures 2b and 2c). During the first 48 hours after the wind was turned off, the topographic wave completed its half cycle as can be seen in Figures 2a–2c, causing a reversal of

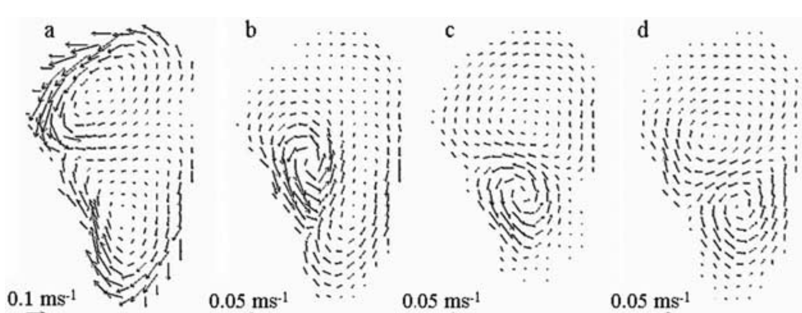

Figure 2. Simulated depth-averaged currents calculated by ROMS driven by a theoretical easterly wind field: (a) 12 hours, (b) 36 hours, (c) 60 hours, and (d) 84 hours after simulation started.

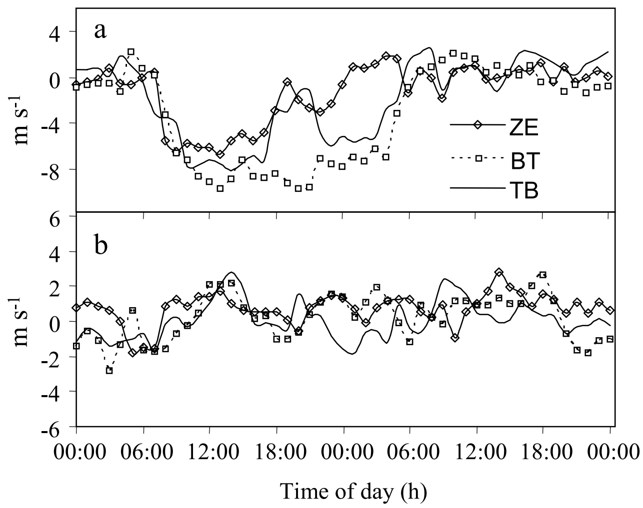

Figure 3. Mean hourly values of (a) east–west and (b) north–south wind components at stations Zemach (ZE), Tabgha (TB), and Beit-Tzeida (BT) during 01–03 January 2001.

the flow at the lake center. Owing to this propagation rate, the expected time period of the basin-scale topographic wave is approximated to be close to four days. If a full cycle is completed, the circulation pattern should be similar to that at the end of the forcing period, although with weaker current magnitudes.

[33] At this time (Figure 2c) the cyclonic gyre covered the southern part of the lake while the anticyclonic gyre spanned the area from the lake center to the northern part of the lake. Since the lake is relatively shallow, there is a substantial effect of bottom friction to slow the dynamics. In the absence of other sources of energy, dissipation reduced the flow magnitude to negligible values after 84 hours (Figure 2d), such that it was difficult to observe the completion of a full cycle of the topographic wave. We estimated the frictional decay time (T_f) using the relation suggested by *Csanady* [1978], $T_f = \frac{h^2}{c_d U}$, where h is the depth (m), c_d is the bottom drag coefficient (0.002), and U the transport ($m^2\ s^{-1}$). In the shallower areas, (less than 8 m) the frictional decay time was approximately 4 hours while at the deepest part of the lake it was 100 hours. The overall average was 43 hours. These findings are in reasonable agreement with the numerical results.

[34] The effect of the bottom friction on the topographic wave frequency has been examined by *Huang and Saylor* [1982] using the linear potential vorticity conservation equation. It was shown that while bottom friction has a substantial effect on current magnitudes, the effect on the wave frequency is minor. We carried out several experiments (results not shown) in which we changed the bottom friction coefficient by an order of magnitude. The results show only a marginal effect on the wave frequency. Similar results were shown by *Raudsepp et al.* [2003] applying both linear and nonlinear numerical circulation models (POM) to the Gulf of Riga, Baltic Sea. Our results are consistent with this conclusion.

4.2. Lake Response to an Easterly Storm 01–03 January 2001 Wind Observations

[35] The possibility of the existence of topographic (vorticity) waves in Lake Kinneret was demonstrated by using an idealized, impulse type, easterly wind field (see section 4.1). Our next step was to identify the response of the lake to the action of a more realistic wind field. Such an event occurred during the period 01–03 January, 2001. Measurements of hourly mean east–west and north–south wind components for this period are depicted in Figures 3a and 3b, respectively. Wind components were measured at stations ZE, BT, and TB. A strong, impulse type wind started to blow above the lake region on 01 January 2001, 0800 (LST). Observations from both ZE and BT stations showed that the wind ceased approximately 12 hours later and was followed by a calm wind for the next 36 hours. Wind values measured at TB station showed however, that this strong wind lasted for 17 hours before cessation. Figures 3a and 3b show that this wind flow was essentially easterly with a small deflection to the north. Several prominent features that may have consequences for the lake's circulation may be inferred from this wind event: (1) the strong wind above the lake started and ceased quite rapidly; (2) the breakthrough of the easterly wind flow was first observed near the southern shore (ZE); and (3) the magnitudes of the measured winds near the northern shore (BT and TB) were generally larger than the winds measured near the southern shore (ZE).

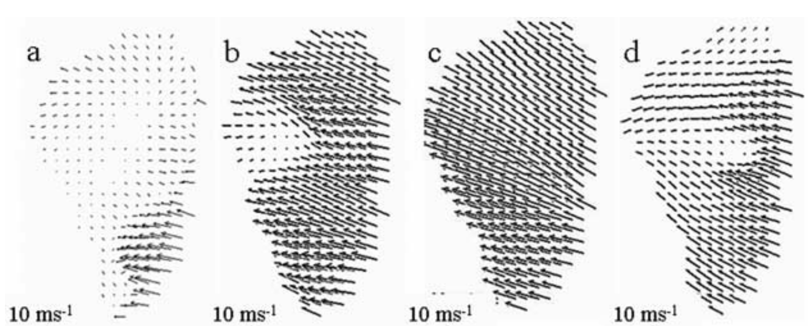

Figure 4. Surface wind fields above the lake at (a) 10 hours, (b) 12 hours, (c) 16 hours, and (d) 24 hours after initiation of a 30-hour RAMS simulation, starting at 0200 LST on 01 January 2001.

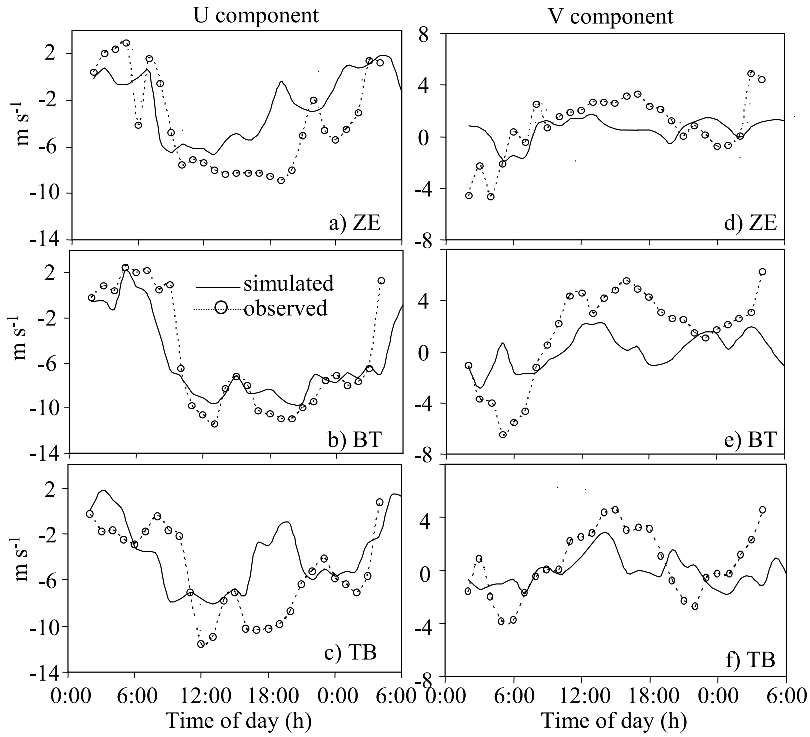

Figure 5. Simulated and observed wind components for 30 hours starting at 0200 LST on 1 January 2001. (a, b, c) The u component at stations ZE, BT, and TB, respectively. (d, e, f) The v component at stations ZE, BT, and TB, respectively.

4.3. RAMS Surface Horizontal Wind Fields

[36] Four representative surface horizontal wind fields (at 10 hours, 12 hours, 16 hours, and 24 hours after the beginning of the simulation), resulting from a 30-hour RAMS simulation (starting at 0200 LST, 01 January 2001) are shown in Figures 4a–4d. The simulated easterly storm penetrated above the lake, first close to its southern shore and later on at its northern shore as shown in Figures 4a and 4b. When the storm covered the entire lake area, the simulated maximal wind magnitudes occurred above its central part. At the southern part of the lake, the wind flow was almost entirely from the east while toward the north, the wind direction became east–south as shown by Figure 4c. This indicates the existence of a wind shear above the lake. Figures 4c and 4d show that the flow magnitude above the northern part of the lake was generally lower than that above the southern. This is not a surprising result although it seems to be in contrast with the station observations. The complex topography that surrounds the lake is a major factor in creating wind variability above the lake. Thus the station observations represent only their immediate vicinity. Both the penetration of the easterly wind at the southern part of the lake and the impulse type of the flow field (as discussed at the end of Methodology) were captured well by the model.

[37] To allow easier comparison between the simulated winds and the observations, both are presented in Figure 5. In general, the airflow features as reflected by the observations are well captured by the model. After the strong wind starts off, the modeled wind magnitude exceeds the observed (see Figures 5a and 5b). It should be kept in mind, however, that the model results were vertically extrapolated to a 10 m height (see section 3.2). We also calculated d, the index of agreement, a statistical descriptive measure of model performance which is defined as

$$d = 1 - \frac{\sum_{i=1}^{n} \left(P_i' - O_i'\right)^2}{\sum_{i=1}^{n} \left(|P_i'| + |O_i'|\right)^2},$$

where n is the number of evaluation points; $P_i' = P_i - \overline{O}$, $O_i' = O_i - \overline{O}$, where P_i is the predicted value, Q_i is the observed value, and $\overline{O}$ is the observed average value. When the predicted values are exactly equal to the observed ones $d = 1$ while when $P_i' = -O_i'$ $d = 0$. In the general case $0 \leq d \leq 1$. The index of agreement, d, was suggested by *Willmott* [1982] to evaluate the accuracy of model prediction. The method is based on a complement of difference and summary univariate indices such as described above. It is an alternative method to the one of using correlation coefficient such as r^2, which was shown to be misleading in evaluating model accuracy, although indicating statistical significance (see *Willmott* [1982] for example). Applications using this method are also provided by *Steyn and McKendry* [1988] and *Palau et al.* [2005]. It was found that d was good for the stronger east–west wind component (d values of 0.79, 0.87, and 0.8 for BZ, Z, and TB, respectively) but of poorer quality for the relatively weak north–south wind components (d values of 0.65, 0.43, and 0.43 for BZ, Z, and TB, respectively). In addition, there was a time shift between

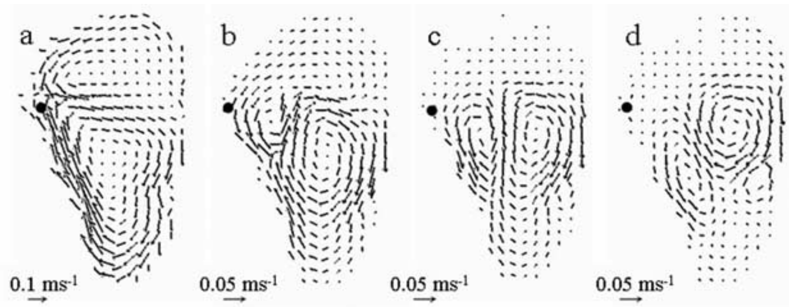

Figure 6. Simulated depth-averaged currents calculated by ROMS driven by RAMS wind fields: (a) 24 hours, (b) 48 hours, (c) 72 hours, and (d) 96 hours after simulation started. The small circle represents the location of current measurements.

the model and the observed wind values. Cross correlation between the simulated and observed wind values indicates that the simulated wind lags the observed wind by 3 hours. Both the breakthrough and the cessation of the simulated strong wind event occurred 3 hours after the observed one. This fact, however, has no effect on the simulation of the lake model; the duration of the simulated strong wind event was consistent with the observed one.

4.4. Simulated Currents

[38] The lake's response to the action of a RAMS simulated easterly wind (see Table 2, Experiment 2) is depicted in Figures 6a–6d. The depth-averaged currents evolved to a double-gyre pattern in response to the wind-forcing (Figure 6a). Similarly to the uniform wind case results (Figure 2), the cyclonic gyre was located between the northern and central part of the lake while the anticyclonic gyre covered the central and southern parts of the lake. The penetration of the wind above the southern part of the lake generated strong currents (high kinetic energy) at a narrow band adjacent to the southern part of the west shore (Figures 6a and 6b). During the transition from the forced to the free period, the gyres started to rotate in a cyclonic sense, exhibiting the properties of a basin-scale topographic wave, with a cyclonic rotation of the current vector in the central deep part of the lake [see *Saylor et al.*, 1980]. During the first 48 hours after the wind was relaxed, the wave completed only one quarter of a cycle (Figures 6a–6c). At this rate, the time period for the basin-scale topographic wave to complete a full cycle should be close to eight days, about twice the topographic wave frequency with uniform wind shown in Figure 2. This phenomenon can be related to the amount of vorticity which is directly introduced into the water from the wind stress field above the lake. We discuss this point further below.

4.5. Comparison Between ROMS Results and Observations in Lake Kinneret, 01–03 January 2001

[39] Evidence for the direct effect of the easterly wind storm is provided from current measurements taken near the Fullya site during winter 2001. The current meter (ADCP) was placed in a very shallow area (7.5 m depth), about 200 m offshore, indicated by a small circle in Figures 6a–6d. The general pattern of the observed and computed depth-averaged current components is shown in Figures 7a and 7b. The observations indicated that the passage of the easterly storm above the lake (first day, 0800 LST) generated a northward current, aligned along the coastline (positive v component, about 3.5 cm s^{-1}, with a smaller negative u component, about 1.5 cm s^{-1}). The above pattern is reasonably well captured by the model (dashed line) with a time lag of several hours (note that all model simulations start from a resting state). Weakening of the wind stress was accompanied by an observed flow reversal, well reflected by the north–south current component, which is also reproduced in the model results. It seems that the current meter was located adjacent to the area where the opposed currents from the south and from the north merged to form the return, upwind, flow, (Figures 6a–6d). In addition, the computed current magnitude decreased monotonically while the magnitude of the observed currents exhibited an oscillatory motion type with a maximal value larger than the forced one (see second day, 1600 LST). The proximity of the current meter to the shore leads us to suspect that other processes, not included in this present work, dominate at

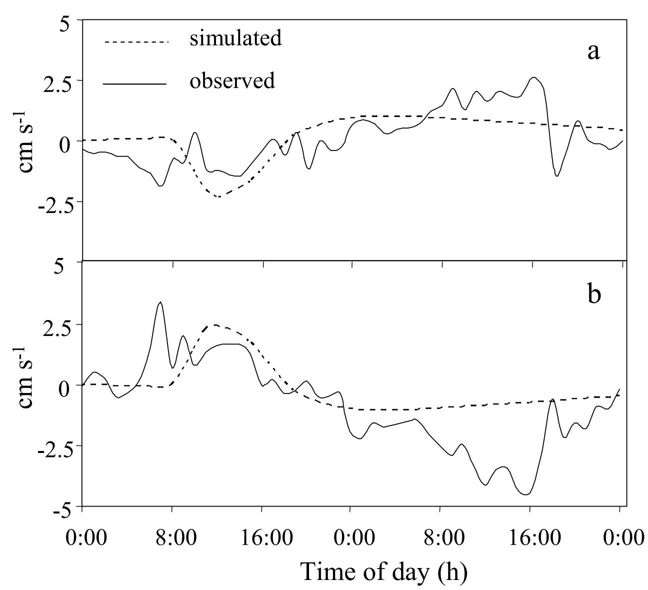

Figure 7. (a) Mean hourly values of observed and simulated (a) east–west and (b) north–south depth-averaged current component near the lake shore at Fullya site for 01–02 January 2001.

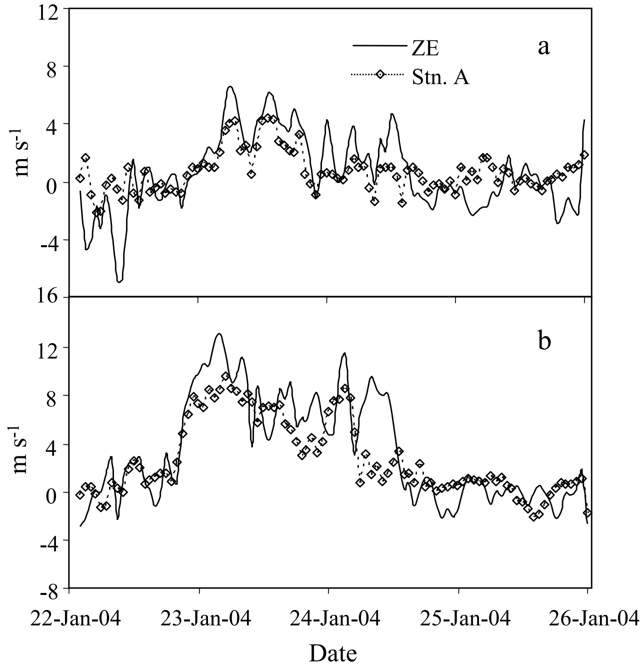

Figure 8. Mean hourly values of (a) east–west and (b) north–south wind components at ZE and Station A during 22–26 January 2004.

this shallow region. Thus the verification of model results using data from this site is limited, especially regarding the topographic wave activity. *Raudsepp et al.* [2003] analyzed the vorticity wave dynamics for the Gulf of Riga, and showed that at regions with a depth between 0 and 9 m, the topographic wave was practically absent. A better verification between observed and modeled results is described below.

4.6. Lake Kinneret Response to a Southwest Wind Storm

[40] As was pointed out above, winter wind storms above Lake Kinneret can occur under the dominance of two characteristic synoptic systems. An example of the lake's response to the passage of the second type wind storm (generated by the passage of a Cyprus low) is described in this section. Figures 8a and 8b show the wind regime that was measured above the center (Station A), and near the southern shore (ZE) of Lake Kinneret for the period 22–26 January 2004. During this period the wind was dominated by the presence of a relatively deep synoptic low above the whole region. The strong wind started to blow from the south (22 January 2004, 2200 LST), slowly rotated in an anticyclonic manner until it finally ceased (24 January 2004, 1400 LST). The wind measurements indicated quite uniform direction with more spatially variable magnitude (Figure 8). For the simulated wind values (see section 4.8.2) the index of agreement, d, was relatively good for the stronger south–north component (0.81, 0.72, 0.63, and 0.27 for Station A, Z, TB, and BZ respectively); less close agreement was found for the mild east–west component (0.46, 0.46, 0.44, and 0.37 for Station A, Z, TB, and BZ, respectively).

[41] We refer to the two numerical experiments that are described in section 3.3 and Table 2, Experiments 3 and 4, respectively, as the 'uniform wind' case (UW) and the 'RAMS simulated wind' case (RW). The resulting circulation patterns and rotation of the double-gyre pattern are depicted in Figures 9 and 10. In general, as a result of the southerly wind, two counterrotating gyres were formed along the major axis (N-S) of the lake (Figures 9b and 10b) and the rotation of the double-gyre pattern was reproduced using the two wind field types (see Figures 9 and 10). However, several differences between the circulation patterns forced by UW and RW are noticeable. Forcing the model with UW fields resulted in a relatively strong northward flow along the west coast accompanied by a return flow directed to the south; the anticyclonic gyre along the west coast was characterized by higher values of kinetic energy than the cyclonic one on the eastern side (Figures 9b and 9c); the two circulation cells formed by using RW were more symmetrical, with a downwind northerly return flow (Figure 10b).

[42] The circulation patterns which are shown in Figures 9c and 10c represent the transition period between the forced and free response of the lake since the strong wind stress relaxes at about 60 hours after initialization. It appears that the propagation speed of the double-gyre pattern formed using RW was higher than that formed by using UW as shown in Figures 9c–9e and 10c–10e. The 48 hours period represented by Figures 9b–9d and 10b–10d, respectively, shows the propagation of the basin-scale topographic wave. During this period, the wave completed approximately one quarter of a cycle when using UW

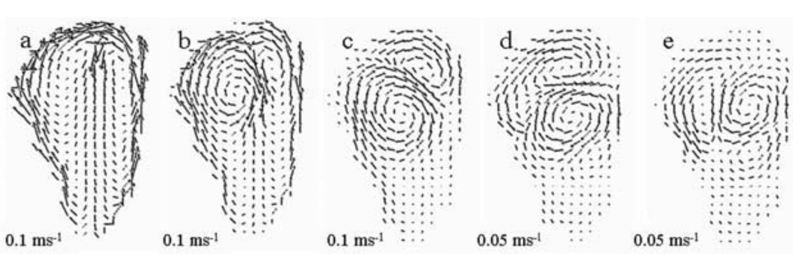

Figure 9. Depth-averaged circulation driven by wind fields from single station observations, UW, (Station A) for 22–26 January 2004: (a) 32 hours, (b) 48 hours, (c) 72 hours, (d) 96 hours, and (e) 120 hours after simulation started.

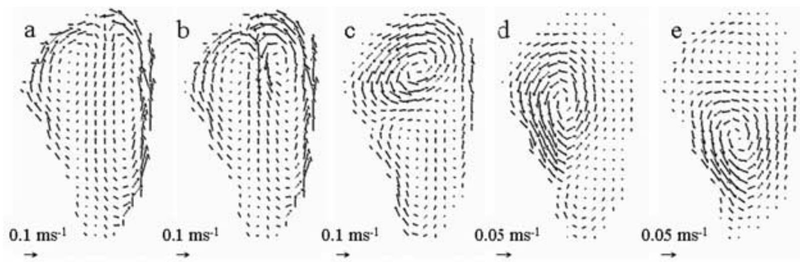

Figure 10. Depth-averaged circulation driven by RAMS-simulated wind fields, RW, for 22–26 January 2004: (a) 32 hours, (b) 48 hours, (c) 72 hours, (d) 96 hours, and (e) 120 hours after simulation started.

forcing, compared to half a cycle for RW forcing. Eventually, for the 72 hours period, depicted in Figures 9b–9e and 10b–10e, the topographic wave completed approximately half a cycle under UW forcing and roughly three quarters of a cycle using RW forcing. We also ran ROMS using a theoretical (spatially and temporally uniform) southerly wind field, which was applied for 12 hours and then terminated. The frequency of the evolving topographic waves (results not shown) was lower than that received when using RAMS simulated winds. This result is another indication that the spatial and temporal variability of the wind field has an important role in the topographic wave frequency.

[43] Another interesting feature that emerged when using RW forcing is that the kinetic energy of the flow which was concentrated initially at the northern cyclonic gyre (Figure 10c) did not disperse but propagated at the wave frequency to the southern part of the lake. When using UW forcing, the kinetic energy of the flow decreased more slowly in the deeper parts of the lake. This however, can be related to the depth configuration of the lake.

4.7. Comparison Between ROMS Results and Observations at Lake Kinneret, 22–26 January 2004

[44] During the relevant period (22–26 January 2004), data was available from a current meter (ADCP) located at Station A (about 43 m depth). We compared the simulated model currents (using both UW and RW wind-forcing) with the observed currents (Figure 11). The RW simulation ended up with a much better agreement with the measured currents. The index of agreement, d, was 0.86 and 0.03 for the RW and UW east–west current components, respectively. For the north–south component a similar value of 0.97 was obtained. The better agreement between the measured and simulated currents resulting from RW forcing is related to the spatial variability of the RAMS simulated wind fields (RW). This can also stand as an indirect validation of the meteorological model results.

[45] A comparison between the measured and simulated currents using uniform wind fields indicates that the mismatch between the two starts at the end of the forcing period (Figure 11a). The observations show that during the first day of the event (22 January 2004) the flow was weak (less than 2 cm s^{-1}) and directed toward the west (see Figures 11a and 11b). The initiation of the strong wind from the south generated a southward current with a small deflection to the west, with a maximal velocity of about 5 cm s^{-1} (Figure 11) on the morning of the second day. This flow can be considered as the return flow. The weakening of the wind (about 60 hours after the beginning of the simulation) was accompanied by a cyclonic rotation of the current vector at the center of the lake, which is an indication of the presence of a topographic wave.

[46] In order to show the cyclonic rotation of the current vector more clearly, we plotted the measured and simulated current vector direction using RW forcing (Figure 12). Two distinct periods can be identified through the time period of the current vector rotation. The first, during the forced period, between 24 hours to 60 hours from the beginning of the simulation, was characterized by a relatively slow change of the current direction, while during the second period, from the second half of the third day onward into the free period (calm wind or no wind at all), the direction of the current vector changed more rapidly.

[47] There are two factors that influence the rotation of the current vector and hence the topographic wave frequency. The first is the rotation of the wind field direction from south to southwest, while the second is the existence of a wind stress curl which introduces vorticity directly

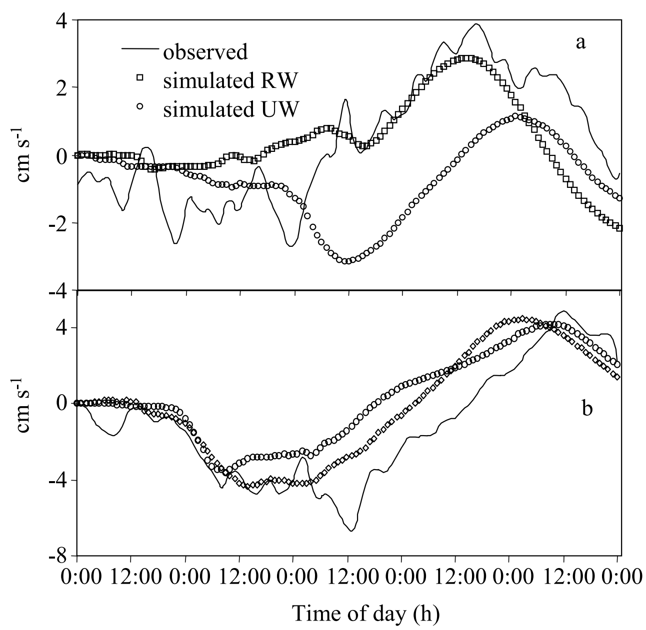

Figure 11. Mean hourly values of observed and simulated using UW and RW (a) east–west and (b) north–south depth-averaged current near the lake center during 22–26 January 2004.

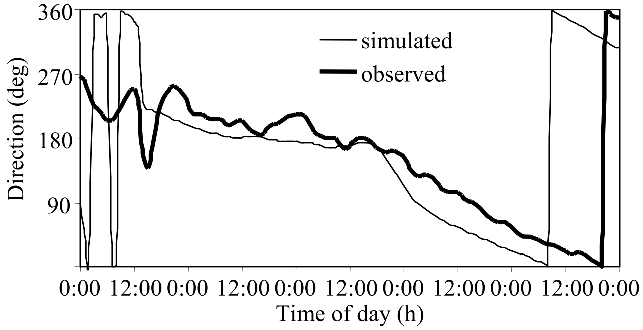

Figure 12. Mean hourly values of observed and simulated using RW depth-averaged current direction near the lake center during 22–26 January 2004.

into the lake. *Raudsepp et al.* [2003] showed that a slow cyclonic rotation of a spatially uniform wind field direction can double the phase propagation of the basin-scale topographic wave. On the other hand, rotation of the wind direction in an anticyclonic manner can act to destroy the wave structure. Our results are in accordance with these results.

4.8. Effect of a Spatially Variable Wind Field

4.8.1. Case I Easterly Wind (Table 2 Experiments 1 and 2)

[48] When forcing the model with uniform wind which obviously does not "inject" vorticity into the water, the topographic wave completes half a cycle in 48 hours. However, when using RAMS simulated wind fields, the averaged (space and time) vertical vorticity of the wind (wind stress curl) was negative (-1.87×10^{-6} s^{-1}), opposing the cyclonic circulation of the topographic wave. This may be the reason for the slower frequency (approximately quarter of a cycle in 48 hours) when using RAMS simulated winds. We note that the wind direction of the simulated wind fields was almost constant in time for this case.

4.8.2. Case II Southwesterly Wind (Table 2 Experiments 3 and 4)

[49] When using uniform wind fields the wave completes a quarter of a cycle in 48 hours, while when using RAMS wind fields, the wave completes half a cycle in the same period. The averaged vertical vorticity of the wind field was positive (3.7×10^{-6} s^{-1}) and the existence of a positive wind stress curl influences not only the formation of a topographic pattern but also its frequency.

4.9. Effect of Wind Stress Curl on the Topographic Wave Frequency

[50] *Ball* [1965] carried out an analytical study on the second class motions of a basin with an elliptic paraboloidal bathymetry given by $z = [(1 - a)x^2 + (1 + a)y^2]/2$ where $-1 \leq a \leq 1$; $a = 0$ is associated with a circular basin. The simplest nontrivial solution was a single circulation cell with constant vorticity (elliptical rotation) in which the water flows along the depth contours. We refer to this solution as the zero mode. The second solution was the first oscillatory mode. The streamlines pattern of this mode depicts two opposing circulation cells which propagate cyclonically around the basin perimeter with a frequency ω_0 given by

$$\omega_0^2 = f^2 \frac{1 - a^2}{49 - 9a^2}, \tag{1}$$

where f is the Coriolis parameter. For Lake Kinnneret $a \cong -0.46$ and therefore the time period of the topographic wave is approximately 7 days. According to the numerical results presented above, the frequency of the double-gyre propagation is affected by the wind field that induced it; the wind stress curl alters the basic frequency of the double-gyre motion. *Ball* [1965] showed that when the first mode interacts with an existing constant vorticity, (Λ, zero mode), the free wave propagation ω_0 becomes

$$\omega_0^{2'} = \omega_0^2 \left[\frac{3}{2}\Lambda(3 + a) + 1\right] \left[\frac{3}{2}\Lambda(3 - a) + 1\right]. \tag{2}$$

Even small values of Λ can significantly alter the double-gyre frequency and consequently the time period of the motion.

[51] It is possible to demonstrate that the vorticity Λ can be induced by the wind stress curl. Basically, when a positive wind stress curl is applied, a cyclonic elliptical circulation is induced that "assists" the cyclonic rotation of the double-gyre pattern; thus a higher double-gyre propagation frequency is to be expected (shorter time period). On the other hand, when a negative wind stress curl is applied, anticyclonic elliptical rotation is induced which "opposes" the cyclonic rotation of the double-gyre pattern. Thus a slower propagation of the double gyre pattern is to be expected. *Ball*'s [1965] results may explain the changes in topographic wave frequency that was observed in our numerical experiments. In case I we had an easterly wind storm with a negative wind stress curl where the double-gyre propagation time period was approximately 8 days. According to equation (2), a constant vorticity, $\Lambda = -0.024$ can induce such a reduction in the frequency ($a = -0.46$ in Lake Kinneret). In case II we had a southwesterly storm with a positive wind stress curl which had a double gyre propagation time period of approximately 4 days. This frequency fits $\Lambda = 0.17$. It is important to note that factors such as depth configuration are also involved in determining the topographic wave frequency. *Saylor et al.* [1980] demonstrated that changing the depth configuration from a parabolic to a conical shape yielded a distinctly different frequency. This finding alone might explain the differences between the results of a numerical model and an analytical one.

5. Conclusions

[52] In this study, numerical experiments using an Oceanic General Circulation Model (OGCM) were carried out in order to study the dynamic response of a medium-sized barotropic lake to different wind-forcing types. All the OGCM experiments exhibited a double-gyre pattern under the action of the wind. The transition to the free period (i.e., weakening of the wind stress) was accompanied by a cyclonic propagation of the double-gyre pattern and closely matched the characteristics of the lowest mode basin-scale

topographic wave obtained by *Ball* [1965]. The free wave decayed owing to the action of friction before completing even one cycle.

[53] When the model was forced with a spatially theoretical homogenous easterly wind field, the estimated time period of the wave was about four days. However, when RAMS-simulated easterly winds were used (case I), the cyclonic propagation of the double-gyre pattern was significantly slower (estimated time period approximately eight days). In case II, the wind fields were determined by the passage of a relatively deep low pressure system above the whole region which led to a strong wind that originated initially from the south to be followed from the southwest. The use of spatially uniform wind fields (but temporally variable according to single station observations) resulted in a slower propagation of the wave (estimated time period of approximately eight days), while a higher propagation rate (estimated time period of approximately four days) was achieved when using RAMS-simulated realistic wind fields.

[54] It is interesting to note that the calculated vertical wind stress curl (spatial-temporal average) was negative in the first case and positive in the second case. This result demonstrates the importance of the wind stress pattern (in particular the wind stress curl) on the structure and frequency of the topographic waves. The physical basis behind this theory is that the curl of the wind field leads to the formation of a single circulation cell in the water body (constant vorticity). This cell interacts with a higher mode two-circulation cell, which is also excited (basin-scale topographic wave) and results in a shift in its frequency. The important concept is that the sign of the wind stress curl determines whether the frequency will increase or decrease. *Huang and Saylor* [1982] suggested that an existing amount of positive elliptical rotation in southern Lake Michigan could be used to explain the gap between observed and calculated time periods. However, this supposition was not related to the role of the wind stress curl. To our knowledge such an example of the importance of wind stress curl on the frequency of the topographic waves has not previously been demonstrated.

[55] The lake model results were validated using observed depth-averaged data at two locations. With RAMS-simulated wind fields, the agreement between the observed and simulated currents is reasonable for the measuring point near the shore and good for the measuring point near the center of the lake. For the simulations described in this manuscript a wind-forcing with a duration of less than two days (magnitude >3 m s^{-1}) was utilized. Using significantly shorter wind duration or longer wind duration ended up with no cyclonic propagation of topographic waves. It seems that this fact is related either to the limited kinetic energy injected to the lake when using too short a duration of wind-forcing, or to the substantial act of bottom friction forces when using longer wind-forcing duration. This point will be examined in more detail in a follow-up study. The presence of a basin-scale topographic wave in our results can explain the phenomenon of flow reversal during the winter as observed by *Serruya* [1975]. Additionally, our results may also explain occasional events of flow reversal during the summer under calm winds. A topographic wave excited by the daily effect of MSB continues as a free propagating wave during the light wind period.

[56] The above numerical findings were also verified using another OGCM (Ocean General Circulation Model, the Massachusetts Institute of Technology general circulation model (the MITgcm) [*Marshall et al.*, 1997a, 1997b] (also A. Adcroft et al., Mitgcm release1 manual, 2002 (online documentation), available at http://mitgcm.org/pelican/online_documents/manual.html). MITgcm is a completely different model (z-coordinate model with finite volume numerical integration). Similar results were obtained using these two OGCMs, a fact that strongly validate our results described above, indicate that the appearance of topographic waves is robust and not model dependent.

[57] **Acknowledgments.** The assistance of field technical and monitoring staff and the database managers at the Kinneret Limnological Laboratory (KLL, Israel) is gratefully acknowledged. We thank A. Nishri from KLL for the current measurements, and the Israeli Meteorological Service for their assistance in wind measurements. Y.A. is supported by the Israeli Center for Complexity Science. The authors thank M. Goldberg for his useful comments and suggestions. This research was supported by the Israel Science Foundation (grant 1319/05) and by the Admiral Yohay Ben-Nun Foundation for Marine and Freshwater Sciences, Israel Oceanographic and Limnological Research Ltd.

References

Alpert, P., and S. O. Krichak (1996), The relative roles of boundaries, initial conditions, and topography in mesoscale simulations of lee cyclogenesis, *J. Appl. Meteorol.*, *35*, 1091–1099.

Alpert, P., A. Cohen, J. Neumann, and E. Doron (1982), A model simulation of the summer circulation from the eastern Mediterranean past Lake Kinneret in the Jordan valley, *Mon. Weather Rev.*, *110*, 106–118.

Antenucci, P. J., J. Imberger, and A. Saggio (2000), Seasonal evolution of the basin-scale internal wave field in a large stratified lake, *Limnol. Oceanogr.*, *45*, 1621–1638.

Asculai, E., E. Doron, and B. Terliuc (1984), Mesoscale flow over complex terrain—A field-study in the Lake Kinneret area, *Boundary Layer Meteorol.*, *30*, 313–334.

Assouline, S., and Y. Mahrer (1996), Spatial and temporal variability in microclimate and evaporation over Lake Kinneret: Experimental evaluation, *J. Appl. Meteorol.*, *35*, 1076–1084.

Avissar, R., and H. Pan (2000), Simulations of the summer hydrometeorology of Lake Kinneret, *J. Hydrometeorol.*, *1*, 95–109.

Ball, F. K. (1965), Second-class motions of a shallow liquid, *J. Fluid Mech.*, *23*, 545–561.

Beckman, A., and D. B. Haidvogel (1993), Numerical simulation of flow around a tall, isolated seamount. Part I: Problem formulation and model accuracy, *J. Phys. Oceanogr.*, *23*, 1736–1753.

Bennett, J. R. (1974), On the dynamics of wind-driven lake currents, *J. Phys. Oceanogr.*, *4*, 400–414.

Birchfield, G. E., and B. P. Hickie (1977), The time dependent response of a circular basin of variable depth to a wind stress, *J. Phys. Oceanogr.*, *7*, 691–701.

Csanady, G. T. (1973), Wind-induced barotropic motions in long lakes, *J. Phys. Oceanogr.*, *3*, 429–438.

Csanady, G. T. (1976), Topographic waves in Lake Ontario, *J. Phys Oceanogr.*, *6*, 93–103.

Csanady, G. T. (1978), Water circulation and dispersal mechanism, in *Lakes: Chemistry, Geology and Physics*, edited by A. Lerman, pp. 21–64, Springer, New York.

Harrington, J. Y. (1997), The effects of radiative and microphysical processes on simulated warm and transition season Arctic stratus, Ph.D. dissertation, 289 pp., Colo. State Univ., Fort Collins.

Huang, J. C. K., and J. H. Saylor (1982), Vorticity waves in a shallow basin, *Dyn. Atmos. Oceans*, *6*, 177–196.

Kain, J. M., and J. M. Fritsch (1993), Convection parameterization for mesoscale models: The Kain-Fritsch scheme—The representation of cumulus convection in numerical models, *Meteorol. Monogr.*, *24*, 165–170.

Large, W. G., J. C. McWilliams, and S. C. Doney (1994), Oceanic vertical mixing: A review and a model with a nonlocal boundary layer parameterization, *Rev. Geophys.*, *32*, 363–403.

Laval, B., J. Imberger, B. R. Hodges, and R. Stocker (2003), Modeling circulation in lakes: Spatial and temporal variations, *Limnol. Oceanogr.*, *48*, 983–994.

Mahrer, Y. (1984), An improved numerical approximation of the horizontal gradients in a terrain-following coordinate system, *Mon. Weather Rev.*, *112*, 918–922.

Mahrer, Y., and R. A. Pielke (1977), A numerical study of the airflow over irregular terrain, *Beitr. Phys. Atmos.*, *50*, 98–113.

Marshall, J., A. Adcroft, C. Hill, L. Perelman, and C. Heisey (1997a), Hydrostatic, quasi-hydrostatic and nonhydrostatic ocean modeling, *J. Geophys. Res.*, *102*, 5753–5766.

Marshall, J., C. Hill, L. Perelman, and A. Adcroft (1997b), Hydrostatic, quasi-hydrostatic, and nonhydrostatic ocean modeling, *J. Geophys. Res.*, *102*, 5733–5752.

Mellor, G. L., and T. Yamada (1982), Development of a turbulence closure model for geophysical fluid problems, *Rev. Geophys.*, *20*, 851–875.

Mysak, L. M. (1985a), Topographic waves in a stratified elliptical basin, with application to the Lake of Lugano, *Philos. Trans. R. Soc., Ser. A*, *316*, 1–55.

Mysak, L. M. (1985b), Elliptical topographic waves, *Geophys. Astrophys. Fluid Dyn.*, *31*, 93–135.

Ou, H. W., and J. R. Bennett (1979), A Theory of the mean flow driven by long internal waves in a rotating basin, with application to Lake Kinneret, *J. Phys. Oceanogr.*, *9*, 1112–1125.

Palau, J. L., G. Perez-Landa, J. J. Dieguez, C. Monter, and M. M. Milan (2005), The importance of meteorological scales to forecast air pollution scenarios on coastal complex terrain, *Atmos. Chem. Phys.*, *5*, 2771–2785.

Pan, H., R. Avissar, and B. D. Haidvogel (2002), Summer circulation and temperature structure of Lake Kinneret, *J. Phys. Oceanogr.*, *32*, 295–313.

Pielke, R. A., et al. (1992), A comprehensive meteorological modeling system-RAMS, *Meteorol. Atmos. Phys.*, *49*, 69–91.

Podsetchine, V., and G. Schernewski (1999), The influence of spatial wind inhomogeneity on flow patterns in a small lake, *Water Res.*, *33*, 3348–3356.

Rao, D. B., and D. J. Schwab (1976), Two dimensional normal modes in arbitrary enclosed basins on a rotating Earth: application to lakes Ontario and Superior, *Philos. Trans. R. Soc., Ser. A.*, *281*, 63–96.

Rao, Y. R., M. J. McCormick, and C. R. Murthy (2004), Circulation during winter and northerly storm events in southern Lake Michigan, *J. Geophys. Res.*, *109*, C01010, doi:10.1029/2003JC001955.

Raudsepp, U., D. Beletsky, and D. Schwab (2003), Basin-scale topographic waves in the Gulf of Riga, *J. Phys. Oceanogr.*, *33*, 1129–1140.

Rhines, P. B. (1969), Slow oscillations in an ocean of varying depth: Part 1. Abrupt topography, *J. Fluid Mech.*, *37*, 161–189.

Rubbert, S., and J. Kongeter (2005), Measurements and three-dimensional simulations of flow in a shallow reservoir subject to small-scale wind field in homogeneities induced by sheltering, *Aquat. Sci.*, *67*, 104–121.

Saylor, J. H., C. K. Huang, and R. Reid (1980), Vortex modes in southern Lake Michigan, *J. Phys. Oceanogr.*, *10*, 1814–1823.

Schwab, D. J., and D. Beletsky (2003), Relative effect of wind stress curl, topography, and stratification on large-scale circulation in Lake Michigan, *J. Geophys. Res.*, *108*(C2), 3044, doi:10.1029/2001JC001066.

Serruya, S. (1975), Wind, water and motions in Lake Kinneret, *Verh. Int. Ver. Limnol.*, *19*, 73–87.

Serruya, S., E. Hollan, and B. Bitsch (1984), Steady winter circulations in Lake Constance and Kinneret driven by wind and main tributaries, *Arch. Hydrobiol.*, *1*, 33–110.

Shchepetkin, A. F., and J. C. McWilliams (2005), The Regional Ocean Modeling System (ROMS): A split-explicit, free-surface, topography-following coordinates ocean model, *Ocean Modell.*, *9*, 347–404.

Simons, T. J. (1980), Circulation models of lakes and inland seas, *Can. Bull. Fish. Aquat. Sci.*, *203*, 68–84.

Song, Y., and D. B. Haidvogel (1994), A semi-implicit ocean circulation model using a generalized topography-following coordinate system, *J. Comput. Phys.*, *115*, 228–244.

Steyn, D. G., and I. G. McKendry (1988), Quantitative and qualitative evaluation of a three-dimensional mesoscale numerical model of a sea breeze in complex terrain, *Mon. Weather Rev.*, *116*, 1914–1926.

Stocker, T. (1988), A numerical study of a topographic wave reflection in semi-infinite channels, *J. Phys. Oceangr.*, *18*, 609–618.

Verhagen, J. H. G. (1994), Modeling phytoplankton patchiness under the influence of wind driven currents in lakes, *Limnol. Oceanogr.*, *39*, 1551–1565.

Willmott, C. J. (1982), Some comments on the evaluation of model performance, *Bull. Am. Soc.*, *63*, 1309–1313.

Wüest, A., and A. Lorke (2003), Small-scale hydrodynamics in Lakes, *Annu. Rev. Fluid Mech.*, *35*, 373–412.

Y. Ashkenazy, Department of Solar Energy and Environmental Physics, Jacob Blaustein Institutes for Desert Research, Ben-Gurion University of the Negev, Sede Boqer Campus, Sede Boqer 84990, Israel.

S. Assouline, Department of Environmental Physics and Irrigation, Institute of Soils, Water and Environment Sciences, Volcani Center, Agricultural Research Organization, Bet Dagan 50250, Israel.

P. Katsafados, Laboratory of Meteorology, Department of Applied Physics, National and Kapodistrian University of Athens, Athens GR-15784, Greece.

Y. Mahrer and E. Shilo, Department of Soil and Water Sciences, Hebrew University of Jerusalem, Rehovot 76100, Israel. (shilo@agri.huji.ac.il)

A. Rimmer, Yigal Alon Kinneret Limnological Laboratory, Oceanographic and Limnological Research, Migdal 14940, Israel.